Bottom interacting sound at 50 km range in a deep ocean environment

Ilya A. Udovydchenkov[a]
Applied Ocean Physics and Engineering Department, Woods Hole Oceanographic Institution, Woods Hole, Massachusetts 02543

Ralph A. Stephen
Geology and Geophysics Department, Woods Hole Oceanographic Institution, Woods Hole, Massachusetts 02543

Timothy F. Duda
Applied Ocean Physics and Engineering Department, Woods Hole Oceanographic Institution, Woods Hole, Massachusetts 02543

S. Thompson Bolmer
Geology and Geophysics Department, Woods Hole Oceanographic Institution, Woods Hole, Massachusetts 02543

Peter F. Worcester and Matthew A. Dzieciuch
Scripps Institution of Oceanography, University of California at San Diego, La Jolla, California 92093

James A. Mercer and Rex K. Andrew
Acoustics Department, Applied Physics Laboratory, University of Washington, Seattle, Washington 98105

Bruce M. Howe
Department of Ocean and Resources Engineering, University of Hawai'i at Manoa, Honolulu, Hawaii 96822

Data collected during the 2004 Long-range Ocean Acoustic Propagation Experiment provide absolute intensities and travel times of acoustic pulses at ranges varying from 50 to 3200 km. In this paper a subset of these data is analyzed, focusing on the effects of seafloor reflections at the shortest transmission range of approximately 50 km. At this range bottom-reflected (BR) and surface-reflected, bottom-reflected energy interferes with refracted arrivals. For a finite vertical receiving array spanning the sound channel axis, a high mode number energy in the BR arrivals aliases into low mode numbers because of the vertical spacing between hydrophones. Therefore, knowledge of the BR paths is necessary to fully understand even low mode number processes. Acoustic modeling using the parabolic equation method shows that inclusion of range-dependent bathymetry is necessary to get an acceptable model-data fit. The bottom is modeled as a fluid layer without rigidity, without three dimensional effects, and without scattering from wavelength-scale features. Nonetheless, a good model-data fit is obtained for sub-bottom properties estimated from the data.
© 2012 Acoustical Society of America. [http://dx.doi.org/10.1121/1.4747617]

I. INTRODUCTION

Understanding the basic physics of sound propagation in the deep ocean and its interaction with the seafloor is one of the most important problems in underwater acoustics. The acoustic energy scattered by topographic features or refracted beneath the seafloor often interferes with direct purely water-column-refracted arrivals, complicating the received signals. This interference imposes limitations on the effectiveness of acoustic methods in many applications. In this paper acoustic bottom interaction in the deep water Long-Range Ocean Acoustic Propagation Experiment [LOAPEX, Mercer *et al.* (2005, 2009)] is analyzed. The LOAPEX experiment was conducted in September–October of 2004 in the eastern North Pacific Ocean. Transmissions from a ship-suspended controlled acoustic source at 800 and 350 m depths were recorded on two moored vertical line arrays (VLAs) in proximity to one another: A shallow vertical line array (SVLA) positioned near the sound channel axis and a deep vertical line array (DVLA) positioned closer to the bottom. The SVLA consisted of 40 hydrophones with 35 m spacing, covering depths between approximately 350 and 1750 m. Only the data collected by the SVLA are considered in this paper, and only a subset of transmissions from approximately a 50 km range is analyzed here. The transmitted signals were phase-modulated *m*-sequences, 1023 digits long with 1 digit equal to 2 cycles of the carrier frequency, either 75 Hz (at 800 m depth) or 68.2 Hz (at 350 m depth). LOAPEX was one of three components of the large North Pacific Acoustic Laboratory 2004 (NPAL04) experiment. The data collected during different phases of the

[a]Author to whom correspondence should be addressed. Electronic mail: ilya@whoi.edu

NPAL04 experiment have been analyzed by various investigators (Van Uffelen *et al.*, 2009, 2010; Chandrayadula, 2009; Udovydchenkov, 2007; Udovydchenkov *et al.*, 2012; Sikora, 2009; Stephen *et al.*, 2008, 2009). However, a data-model comparison of absolute amplitudes and absolute travel times of bottom-reflected (BR) arrivals has not been previously considered. The present paper is a step toward fully understanding the influence of local bathymetric features and sub-bottom properties on the acoustic arrival pattern.

The approach presented in this paper is conceptually similar to the one given by Heaney (2004a,b). He developed a method of rapid geoacoustic characterization in shallow water from three derived quantities: The slope of the striation pattern in the range-frequency domain, the frequency spacing of the striations, and the slope of the incoherent transmission loss with range. The misfits between the data and the model predictions for these quantities were combined to construct an objective (cost) function. The minimization of the cost function provided a good estimate of sediment properties. The method in this paper is also based on minimizing a cost function constructed from the data-model misfit, and a similar sediment model is used. Advances in experimental deep ocean acoustics have made it possible to use absolute intensities and absolute travel times as observable quantities in the construction of the cost function. Here, to estimate the sediment properties the misfit of acoustic intensity between the data and the model is computed. The misfit is minimized by using a "brute-force" search through the sediment parameters. The main focus of this work is to understand the physical processes involved in long-range sound propagation between sources and receivers in the water column. It is shown for 50 km ranges and relatively shallow sources and receivers that seafloor topography and sub-bottom properties affect the purely water-column-refracted arrival structure. The inversion method presented estimates seafloor properties that are useful in predicting the performance of similar experiments. The main differences in this paper from prior work on bottom inversion are: (a) The method is applied to deep water conditions, (b) the data were acquired on a VLA, (c) the source was at a single range about a convergence zone away, and (d) because absolute intensity levels and absolute travel times were recorded, the misfit was defined in terms of acoustic wave field intensity differences in the depth-time domain.

The remainder of the paper is organized as follows. In Sec. II the statement of the problem and the motivation for this study are presented. Section III shows the results of the geoacoustic inversion. The conclusions and limitations of this analysis are summarized in Sec. IV.

II. BOTTOM-REFLECTED ARRIVALS IN LOAPEX

The interference of direct purely water-column-refracted arrivals and BR energy is illustrated in this section using modal analysis of acoustic receptions. BR arrivals observed in the LOAPEX transmissions from station T50 are shown and compared with preliminary numerical model predictions. Two bottom models are chosen for the simulations. A third model, the result of the inversion procedure described in

Sec. III, is also shown in order to demonstrate the improvement in fit over the preliminary models and to describe the ray paths that contribute to the total field at a 50 km range. The first model has a range-independent topography with homogeneous bottom properties (compressional sound speed, attenuation, and density). The second model has real topography, constructed from multibeam bathymetry surveys and from satellite-derived bathymetry (Smith and Sandwell, 1997), with bottom properties similar to the ones described by Stephen *et al.* (2009), which were based on a general knowledge of the Pacific seafloor. It is concluded that both numerical simulations show a significant mismatch with the observed intensities (1080% mismatch for the flat, homogeneous bottom, and 480% mismatch for the more realistic bottom with measured topography). The simulation based on the third model shows a much better fit (74% mismatch).

A. Acoustic wave field simulations

For long-range sound propagation in the deep ocean, acoustic propagation models based on the parabolic equation approximation are computationally efficient and handle range-dependence naturally. A geometric ray-based solution is also used here for qualitative illustrations, but it is not suitable for quantitative predictions, as discussed further in Sec. II C. There are other, less convenient, methods. The normal mode approach (Jensen *et al.*, 2000) is computationally intensive in range-dependent environments. In a deep ocean the normal mode approach would require computation of broadband range-dependent bottom interacting modes together with all mode coupling coefficients. Finite difference and finite element methods require too much computational time for the ranges and frequencies being considered.

To construct numerically simulated wave fields, the range-dependent acoustic propagation model (RAM) (Collins and Westwood, 1991; Collins, 1993) was used. A single range- independent sound-speed profile was constructed from environmental measurements made at the VLA location. Internal-wave-induced sound-speed perturbations were modeled using the procedure described by Colosi and Brown (1998). The strength of the internal-wave-induced perturbations was chosen to be one nominal Garret–Munk strength (1 GM). The internal-wave-induced perturbation field was superimposed on top of the background sound-speed profile. The RAM model allows computation of absolute transmission loss. With knowledge of the source level [given in Mercer *et al.* (2005)], absolute values of intensity can therefore be computed and compared with measured intensities. The acoustic source spectrum was chosen to have the shape of a Hanning window with the peak at $f_0 = 75$ Hz and zeros at $f_0 - f_0/4$ and $f_0 + f_0/4$, approximating the spectrum of the LOAPEX source. The range step used in the RAM simulations was 19.75 m, and the depth increment was 1 m. The bathymetry was sampled every 79 m. The bottom properties used in the simulations are summarized in Table I.

B. Modal analysis of the LOAPEX data

The work presented in this paper was largely motivated by the modal analysis of the LOAPEX data, which showed

J. Acoust. Soc. Am., Vol. 132, No. 4, October 2012

Udovydchenkov *et al.*: Bottom reflections in a deep ocean   2225

TABLE I. Summary of bottom properties used in Simulations A, B, and C. Here "S&S + swath" is a topographic profile constructed from swath bathymetry measurements made during the experiment and from satellite-derived bathymetry (Smith and Sandwell, 1997). The horizontal resolution is approximately 80 m. Here z denotes depth in meters, dz is the thickness of a layer, c is the compressional sound speed, α is the attenuation, and ρ is the density. Subscripts "s" and "b" denote "sediment" and "basalt."

Bottom properties	Bathymetry	dz_s (m)	c_s (km/s)	α_s (dB/λ)	ρ_s (g/cm^3)	dz_b (m)	c_b (km/s)	α_b (dB/λ)	ρ_b (g/cm^3)
Simulation A	Flat	∞	1.6	0.2	1.35	–	–	–	–
Simulation B	S&S + swath	20	1.6	0.2	$1.35 + \frac{1.8-1.35}{300} \times z_s$	2000	$4 + 0.0014 \times z_b$	0.05	$1.91 + 0.158 \times c_b$
Simulation C	S&S + swath	50	1.49	0.5	1.35	1000	$4 + 0.0014 \times z_b$	0.05	$1.91 + 0.158 \times c_b$

the interference of purely water-column-refracted signals with bottom reflections (Udovydchenkov *et al.*, 2012). It was noted that the bottom properties used in the model, such as bathymetry, sediment thickness, compressional sound speed, and attenuation, significantly influence not only intensities and arrival times of BR signals, but also the data-model comparison of low-order modal arrivals (with mode numbers $m_0 \lesssim 10$). In a typical mid-latitude deep ocean environment, these low-order modes are trapped near the sound-channel axis (which is at about 1 km depth), and their propagation and scattering should not be sensitive to the ocean bottom properties. However, because of finite spacing between SVLA elements, the energy in high-order bottom-interacting modes ($m \gtrsim 100$) aliases into low-order modes, thus complicating the observed arrival structure. This phenomenon is illustrated in Fig. 1. In Fig. 1 the data collected during trans-

missions from a broadband source deployed at 350 m depth, at 44.714 km range from the SVLA (T50), and with the carrier frequency of 68.2 Hz are analyzed and compared with propagation model predictions. The upper row [Figs. 1(a)–1(c)] shows absolute intensities of time fronts, the wave fields as functions of absolute travel time and depth. Here Fig. 1(a) is the LOAPEX data coherently averaged over all transmissions (approximately 7 h of transmission time with gaps), Fig. 1(b) shows the RAM simulation with range-independent topography and constant values of bottom properties (compressional sound speed, attenuation, and density) as in Simulation A discussed later in Fig. 4, and Fig. 1(c) shows the RAM simulation based on the results of the inversion procedure described in Sec. III (the same bottom as in Simulation C in Fig. 4). The bottom row of Fig. 1 shows modal arrivals for mode numbers $m = 0$, 1, and 9
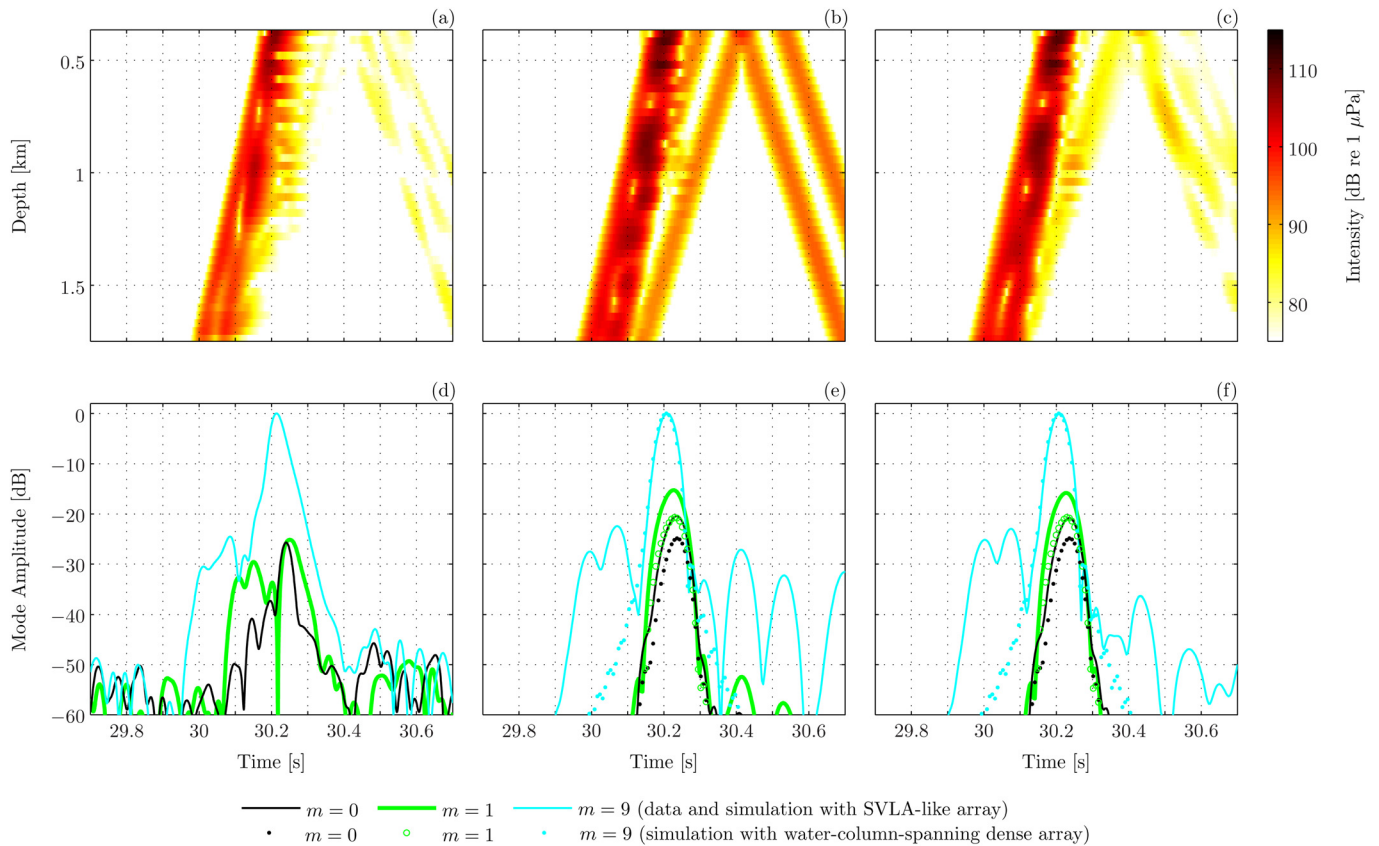

FIG. 1. (Color online) Comparison of broadband acoustic wave fields at T50 for a source at 350 m depth and center frequency of 68.2 Hz in the depth-time domain (top row) and as mode-processed wave fields (bottom row). The left column is observed LOAPEX data [(a) and (d)]. The middle column is a model prediction with a homogeneous bottom and flat topography [(b) and (e)]. The right column is a model prediction with the best-fit bottom properties obtained in Sec. III [(c) and (f)]. The bottom row shows modal arrivals for modes $m = 0$, 1, and 9 with an SVLA-like receiving array (solid lines) and with a dense water-column-spanning receiving array (dots).

corresponding to the data and the two simulations. The details of the mode processing are described by in Udovyd-chenkov et al., (2012). Note that the mode-processed data fields [shown in Fig. 1(d)] were coherently averaged over the entire duration of transmissions from T50 with the source at 350 m. The solid lines show the processing results using either the actual SVLA array data [Fig. 1(d)], or an array that mimics the SVLA aperture and hydrophone spacing [Figs. 1(e) and 1(f)]. The dotted lines in Figs. 1(e) and 1(f) show processing results of simulated wave fields using a dense water-column-spanning array (5 m spacing).

Several interesting observations can be made from Fig. 1. First, recall that if the shape of the spectrum of the source is Gaussian (or nearly Gaussian, which is the case for these LOAPEX transmissions), then modal arrival amplitudes on a logarithmic scale look parabolic. The distortions to the para-bolic shape of these arrivals due to dispersion and scattering at this short range are small (Udovydchenkov et al., 2012). These idealized Gaussian-like arrivals are well predicted by the numerical model with the dense receiving array [dotted lines in Figs. 1(e) and 1(f)]. With the existing array geometry, however, BR energy aliases into low-order modes as seen in all three bottom panels. Some of that energy can be "time-gated" (for example, arrivals past 30.35 s), but some energy overlaps with and even arrives earlier than the main arrival (such as energy between 29.9 and 30.1 s). The BR arrivals produce a "signal-generated noise" that dramatically reduces the effective signal-to-noise ratio (SNR). As seen from Fig. 1(d), the real SNR in the data can be as high as 50 dB (for $m = 9$). To properly interpret low-order modal arrivals with amplitudes between 25 and 50 dB below the peak value it is necessary to consider the effect of the aliased bottom arrivals. To fully understand the *observed* structure of modal arrivals, knowledge of bottom properties is therefore required.

The second observation in Fig. 1(d) is that the excitation levels of modes $m = 0$ and $m = 1$ are almost the same. In reality this should not be the case because the source at 350 m depth excites modes $m = 0$ and $m = 1$ via exponential "tails" of the modal eigenfunctions. Excitation amplitudes should be proportional to the modal eigenfunction ampli-tudes squared at the source depth. This is indeed the case with the simulations. So, another conclusion is that knowl-edge of bottom properties is important for studying levels of excitation of low-order modes and redistributions of energy among low-order modes due to scattering along the propaga-tion path. Unfortunately, the simulations shown in Figs. 1(c) and 1(f) with the "best-fit" bottom properties (discussed in Sec. III) also show that mode $m = 1$ is excited stronger than mode $m = 0$, suggesting that other effects, such as bottom shear or out-of-plane scattering, could be important. The best-fit model, however, results in significant improvement (at least qualitative) in the arrival structure, both in the depth-time domain and the time-mode number domain for arrival energy past 30.3 s.

C. Geometry of acoustic arrivals at the receiving array

The analysis presented in the rest of this paper will be carried out with the source deployed at 800 m with a 75 Hz

center frequency. The technique can also be applied to the data with the source at 350 m depth with slight modifications but the analysis with the deeper source is simpler. With the source placed close to the sound-channel axis, low-order modes (the energy corresponding to the latest purely water-column-refracted arrivals) are strongly excited, and it is eas-ier to separate purely water-column-refracted arrivals from bottom reflections.

Before discussing the agreement between the data and the model, the basic geometry of sound propagation to the receiving array (SVLA) is described. For numerical model-ing the water-column environment was the same as described in Sec. II A. The bottom properties were chosen to be the same as those used for Simulation C (discussed in Sec. III; see Table I for the summary of bottom properties). Figure 2 illustrates the formation of the arrival pattern at the SVLA. The left panel shows the single-frequency (75 Hz) RAM- simulated transmission loss as a function of range and depth with eight different geometric rays, obtained using the EIGENRAY code (Dushaw and Colosi, 1998), superim-posed. These eight rays were chosen such that each of them demonstrates qualitatively different behavior along the prop-agation path. Rays shown with filled (empty) symbols have positive (negative) launch angles. Most of these rays can also be differentiated by the number of turning points between the source and the receiver. For example, the ray shown by filled diamond symbols has an index +4 (indicat-ing that the launch angle is positive and the ray has 4 turning points). The right panel of Fig. 2 shows the corresponding broadband wave field at the receiver range as a function of depth and time. The arrival time and depth for the eight rays are also shown on the right panel using the same notation.

Comparison of the two rays with index −1 (small and large empty circles) shows that although their arrival times and depths are close to each other, their reflection points at the seafloor are over 5 km apart. This is due to the hill in the topography at a 30 km range, which is about 700 m high. The energy in a small region of a time front may contain contributions from different places at the bottom (with potentially different properties).

The hill at 30 km also causes a "split" of the time front branch formed by rays with the index +2 (black filled circles). The hill causes most of the energy forming this time front branch to arrive earlier than if there were no hill. Some energy, however, is still reflected at mid-range forming the latter part of this branch. This "split time front" is clearly visible in the LOAPEX data but, of course, cannot be simu-lated with range-independent topography.

In order to estimate the domain of influence on the sea-floor that contributes to the BR and surface-reflected, bottom-reflected arrivals measured by the SVLA, a large number of rays were traced, and those rays that fell within the SVLA vertical aperture were selected. The domain of influence, i.e., those parts of the seafloor that contribute to the arrival pattern at the SVLA, are shown by shading of the sediment layer in the left panel of Fig. 2. The magnified region is shown in Fig. 3. This domain consists of two parts with ranges of 13.4 to 26.3 km (covering approximately mid-range distances) and 28.5 to 31.0 km (covering the top-left

J. Acoust. Soc. Am., Vol. 132, No. 4, October 2012

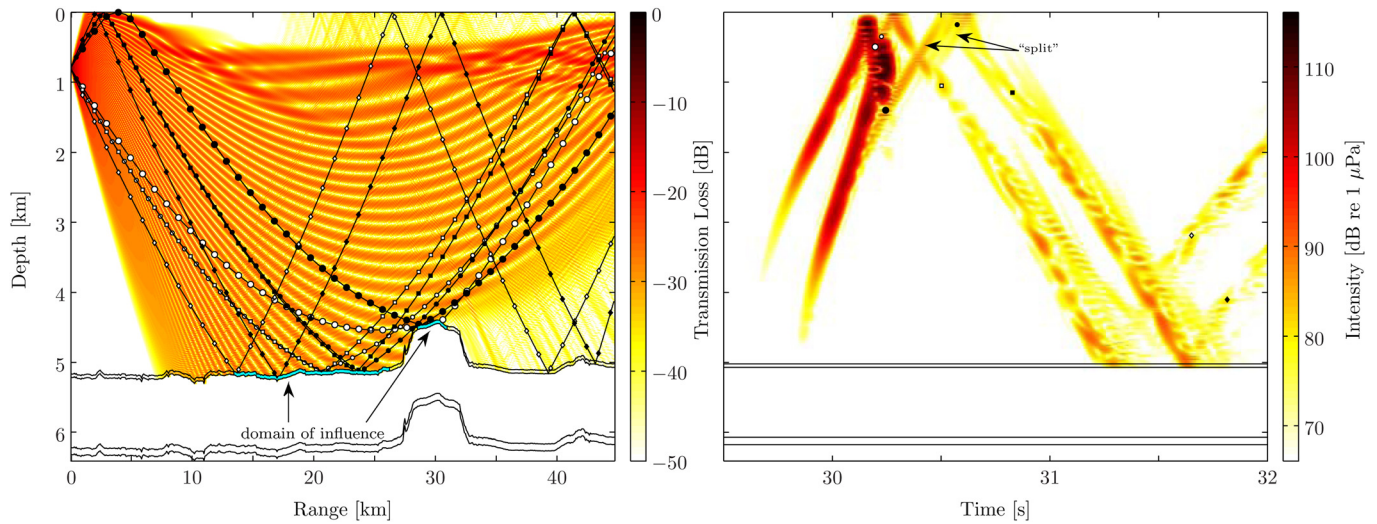Udovydchenkov et al.: Bottom reflections in a deep ocean   2227

FIG. 2. (Color online) Left panel: Single-frequency (75 Hz) RAM-simulated relative transmission loss as a function of depth and range for a source at 800 m. Eight BR geometric rays with qualitatively different behavior are shown using different line styles. The bottom layers, as described in the text and in Table I, are shown with black solid lines. The domains of influence (those points on the seafloor, which contribute to the arrivals recorded by the SVLA) are shown by the shaded region in the sediment layer (see also Fig. 3). Right panel: Simulated time fronts of broadband acoustic pulses with a center frequency of 75 Hz in the same environment as shown on the left panel. The arrival times and depths of the rays shown on the left panel are also shown on the right using a consistent notation. The split of the arrival time front branch is shown by arrows.

side of the hill). Figure 3 also shows the details of the geometric ray trajectories near the seafloor. Geometric rays are not used in this paper for quantitative analysis. A realistic ray-based solution would require smoothing of the bathymetry over a horizontal Fresnel zone width. The horizontal Fresnel zone width estimated using Eq. (15) in Rypina and Brown (2007) for the ray with an upward launch angle of approximately 18.2° (shown by filled small circles) is approximately 1.5 km at the seafloor. In an environment with bathymetry sampled every 79 m, the geometric rays often contribute to different parts of the resulting wave field due to reflections from small facets in the water/sediment or sediment/basalt interface. Nevertheless, the rays are useful in explaining the various features in the observed time fronts.

The band of launch angles for rays penetrating into the sediment layer can be estimated using Snell's law. All rays with launch angles (at 800 m depth) less than about 16.5° do not interact with the bottom. All rays with launch angles below approximately 68.3° cannot penetrate into the high sound speed basalt layer. Since the time fronts considered in this paper are composed of rays with launch angles of less than approximately 25° and the maximum steepness of the topographic profile (after smoothing over the Fresnel scale length) does not exceed 20°, rays that penetrate into the basalt layer do not contribute to the resulting wave field. All bottom-interacting energy that is observed is therefore reflected from either the water/sediment or the sediment/basalt interface.
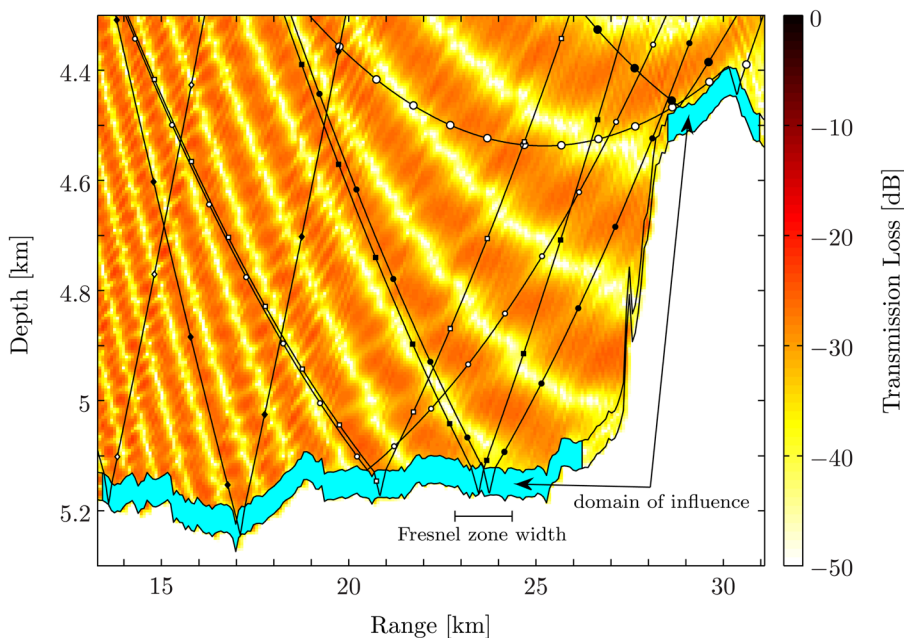

FIG. 3. (Color online) Magnified region from the left panel of Fig. 2 showing the domain of influence and the interaction of geometric rays with the seafloor. The horizontal Fresnel zone width at the seafloor is approximately 1.5 km for the ray shown by small filled circles.

D. Data-model misfit

In this section an example of the measured acoustic wave field from LOAPEX [Fig. 4(a)] is compared with numerically simulated wave fields for three different bottom structures [Figs. 4(b)–4(d)]. The wave field in all cases is displayed as absolute, not relative, intensities. Figure 4(a) shows a typical (of 30 total available) acoustic wave field obtained by coherent averaging over 5 min (i.e., 11 replications of the transmitted signal). Figure 4(b) (Simulation A) shows the numerically simulated wave field using the method described in Sec. II A with flat topography and constant bottom properties. The bottom depth was set to the depth at the SVLA location (approximately 5020 m). Figure 4(c) (Simulation B) shows the numerically simulated wave field in the same water-column environment, but with the real topography discussed in Sec. II and bottom properties that are summarized in Table I. An "artificial" semi-infinite strongly-absorbing layer with attenuation of $\alpha = 10 \, \text{dB}/\lambda$ (where λ is the wavelength) was added below the basalt layer in the RAM numerical model for stability of the solution. All bottom properties are given with respect to the local seafloor depth, i.e., a "bathymetry-following" bottom model was used. Simulation C, obtained using best-fit bottom properties, is discussed in Sec. III.

Comparison of the received signals at 500, 1000, 1250, and 1500 m depths with Simulations A and B reveals a significant mismatch in the BR arrival structure past approximately 30.3 s, both in arrival times of the peaks and intensity levels (Fig. 4). Inspection of Fig. 4 indicates that inclusion of range-dependent topography and realistic bottom properties reduces the data-model misfit. However, a quantitative measure of the goodness of the data-model fit is needed.

While there are many options available to construct the cost function [e.g., Heaney (2004a,b)], in this study the cost function is based on the energy misfit in time and depth between the data and the model. First, a domain in time and depth is defined that contains most of the BR energy but with as little overlap as possible with the water-column refracted arrivals (Fig. 4). Even for the case considered in this paper, this condition cannot be satisfied exactly. Only stable, strong BR arrivals are included in this domain, thus constraining it in time. After the domain was constructed, a manual inspection confirmed that the BR arrivals of interest are contained within the domain for all transmissions.

The received levels (RLs) within the domain are converted to intensities

$$I = 10^{\text{RL}/10}, \tag{1}$$

and the absolute and relative data-model misfits are defined as

$$\Delta = \sum_N |I_{\text{data}} - I_{\text{model}}| \tag{2}$$

and

$$\delta = \frac{\Delta}{\sum_N I_{\text{data}}}, \tag{3}$$

respectively. Here N is the total number of sample points within the domain of interest. The mean value of the misfit for each simulation is defined as the average misfit with respect to the 30 wave fields available from LOAPEX. To
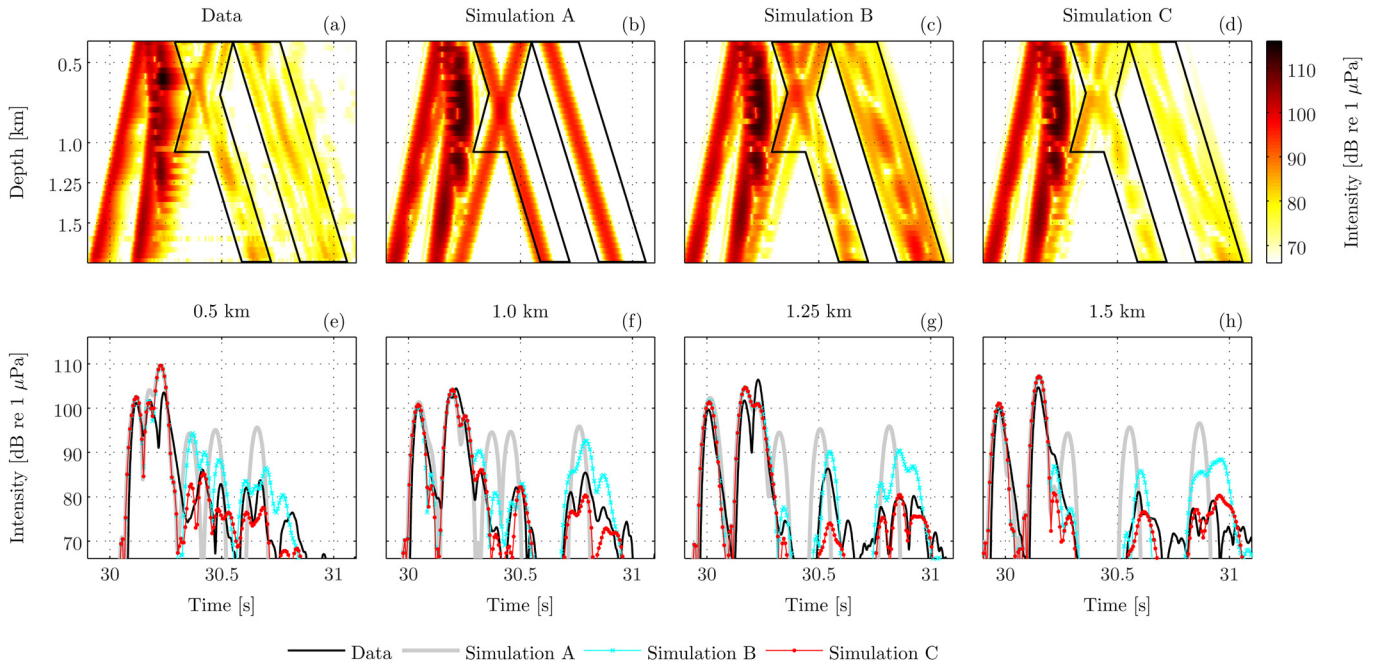

FIG. 4. (Color online) The observed wave field recorded during one of the 5 min LOAPEX transmissions from T50 with the source at 800 m depth (a) is compared with simulations made assuming flat topography and uniform bottom properties (b), real topography and more realistic bottom properties as described in Table I (c), and real topography with the best-fit bottom properties as described in Table I (d). Black solid lines in the upper four panels outline the domain that includes most of the BR energy and is used for computation of the data-model misfit. The lower four panels show data-model comparisons of acoustic intensities at 500, 1000, 1250, and 1500 m depths [(e)–(h), respectively]. The mean relative misfit (defined in the text) between the data and Simulation A is $\delta = 10.8 \pm 2.0$; between the data and Simulation B is $\delta = 4.8 \pm 1.0$; and between the data and Simulation C is $\delta = 0.74 \pm 0.06$.

estimate the errors in the misfit, the 90% confidence interval is determined as 1.645 times the standard deviation computed for all misfits for a particular numerical simulation (assuming a normal distribution). For the two numerical simulations A and B, the relative misfits are $\delta = 10.8 \pm 2.0$ and $\delta = 4.8 \pm 1.0$, respectively. Note that the relative misfit δ in Eq. (3) is unity when the model wave field is identically zero.

As expected, the bottom-interacting arrival structure at this site is least accurately modeled using range-independent bathymetry with a minimally structured bottom. Even if one is interested in purely water-column refracted energy (to the left of the outlined domain in Fig. 4), the arrival pattern is distorted by the interference from bottom-interacting energy, as discussed in Sec. II B. Simulation B with the real bathymetry and a somewhat more complex bottom structure fits better. The influence of the bathymetry alone is shown in Sec. II C to account for several features in the arrival structure that cannot be explained using a flat seafloor. A further significant reduction in the misfit is next obtained in Sec. III using a set of bottom parameters estimated from geoacoustic inversion.

III. GEOACOUSTIC INVERSION

Now a set of bottom parameters is estimated from the data by performing forward simulations for different bottom models and selecting the model that minimizes the misfit

[Eq. (3)]. In order to reduce the parameter space, the model uses real bathymetry but consists of only three layers: The top layer represents sediment, the second layer represents basalt, and the third layer is an artificial absorbing layer used in the numerical model for stability. All layers are bathymetry-following, i.e., their properties are given with respect to the local seafloor depth. The basalt layer is assumed to be the same in all simulations (Table I). Sediment thicknesses were varied from 10 to 100 m in 10 m increments. The compressional sound speed, density, and attenuation were assumed to be constant within the sediment layer. Compressional sound speeds were varied from 1.48 to 1.6 km/s in 0.01 km/s increments, attenuation values were 0.05, 0.1, 0.2, 0.3, 0.4, 0.5, and 0.6 dB/λ, and the density was 1.35 g/cm^3. The results of the inversion are insensitive to the value of density. The bottom parameters that resulted in the minimum mean relative misfit are: $dz = 50$ m, $c_p = 1.49$ km/s, and $\alpha = 0.5$ dB/λ (Fig. 5). The misfit for these parameters is $\delta = 0.74 \pm 0.06$, which is a factor of 6 improvement over Simulation B. The relative misfit as a function of sediment thickness, compressional sound speed, and attenuation, with other parameters held constant, is also shown in Fig. 5. The misfit surface is broad around the minimum and has multiple extrema. There is therefore no guarantee that the minimum found in the above procedure is a global minimum. However, some useful conclusions can still be made. For example, one can estimate the range of parameters for which the relative misfit does not exceed a threshold. If the threshold is set to 1.0, the range of
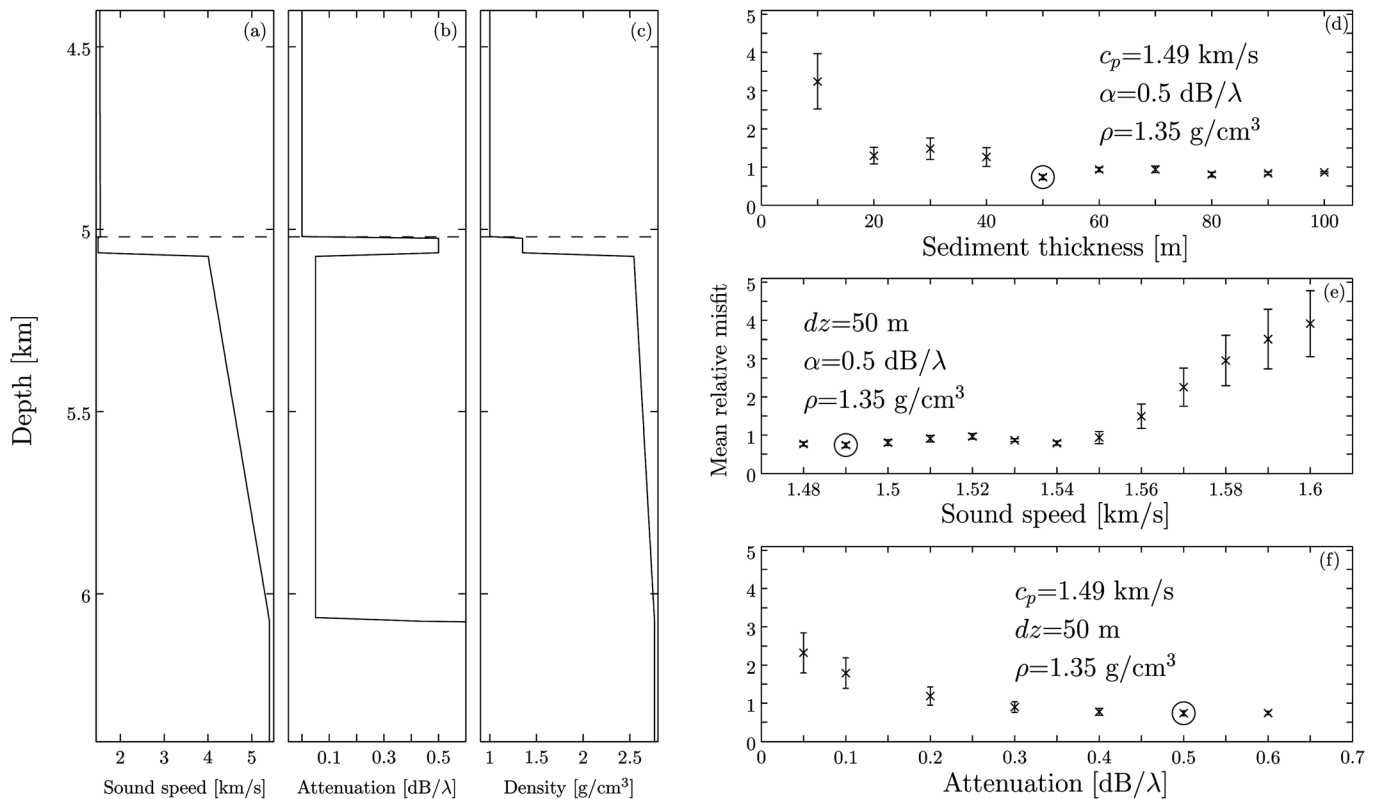

FIG. 5. (a)–(c) Compressional sound speed, attenuation, and density profiles in the sub-bottom obtained from minimization of the mean relative misfit. Values below the sediment are assumed, i.e., not obtained by inversion. Horizontal dashed lines show the seafloor depth at the SVLA location. (d)–(f) Two-dimensional slices of the relative misfit surface as a function of sediment thickness, compressional sound speed, and attenuation. Mean relative misfit is shown together with 90% confidence intervals. The best-fit bottom parameters are shown by circles.

parameters that satisfy this criterion is $dz \geq 30$ m, $c_p \leq 1.55$ km/s, and $\alpha \geq 0.2$ dB/λ. The estimated sediment thickness is in the range reported by Diachok *et al.* (1986) and Stephen *et al.* (1997) for the North Pacific, i.e., generally less than 100 m.

The simulations neglect out-of-plane scattering, shear effects, seafloor fine-scale roughness, and roughness of the sediment/basalt interface. A constant thickness sediment layer with constant properties is also a restrictive assumption. Inclusion of these missing features may shift the best-fit values toward a thinner sediment layer, a higher compressional sound speed, and a smaller attenuation as reported by Bowles (1997).

We also considered a compressional sound-speed gradient of $1\,\text{s}^{-1}$ in the sediment layer. Although this assumption is physically more realistic (Hamilton, 1980), introduction of a gradient only leads to slight changes in arrival times. This result is not surprising because all the energy that penetrates into the sediment reflects off the sediment/basalt interface.

IV. DISCUSSION

In this paper a stable set of BR acoustic arrivals observed in transmissions from approximately 50 km range to a 1400-m long vertical receiving array in deep water are shown to be sensitive to bottom topography and properties. An order of magnitude improvement in the data-model fit is obtained using measured range-dependent bathymetry together with bottom properties estimated from the data. Furthermore, at least one feature in the observed data, the split arrival in Fig. 2, requires a range-dependent model. The range of sub-bottom properties that provide a good model-data fit is, however, quite large.

The inversion done here included internal-wave-induced sound-speed perturbations. Only very minor changes were observed in the structure of the arrival pattern influenced by the bottom in simulations without internal waves. At this short range, high-angle bottom-interacting energy has little interaction with internal-wave-induced perturbations, which are concentrated primarily above the sound channel axis (approximately in the upper 700 m).

Finally, the bathymetric data show that there is a higher hill to the north (around $r = 30$ km) that is not in the source-receiver plane. The bottom reflection, which is modeled in this work as an in-plane reflection off the top of a hill, in reality could have occurred off the side of the out-of-plane hill. Three-dimensional effects could potentially be important.

Bowles, F. A. (**1997**). "Observations on attenuation and shear-wave velocity in fine-grained, marine sediments," J. Acoust. Soc. Am. **101**, 3385–3397.

Chandrayadula, T. K. (**2009**). "Mode tomography using signals from the long range ocean acoustic propagation experiment (LOAPEX)," Ph.D. thesis, George Mason University, Fairfax, Virginia.

Collins, M. (**1993**). "A split-step Padé solution for the parabolic equation method," J. Acoust. Soc. Am. **93**, 1736–1742.

Collins, M. D., and Westwood, E. K. (**1991**). "A higher-order energy-conserving parabolic equation for range-dependent ocean depth, sound speed and density," J. Acoust. Soc. Am. **89**, 1068–1075.

Colosi, J. A., and Brown, M. G. (**1998**). "Efficient numerical simulation of stochastic internal-wave-induced sound speed perturbation fields," J. Acoust. Soc. Am. **103**, 2232–2235.

Diachok, O. I., Dicus, R. L., and Wales, S. C. (**1986**). "Effects of upper crustal geoacoustic parameters on low frequency sound," in *Proceedings of the Symposium on Ocean Seismo-Acoustics*, SACLANT ASW Research Centre, Vol. 16, pp. 711–720.

Dushaw, B. D., and Colosi, J. A. (**1998**). "Ray tracing for ocean acoustic tomography," Technical Report, Applied Physics Laboratory, University of Washington, Seattle, Washington, APL-UW TM 3-98.

Hamilton, E. L. (**1980**). "Geoacoustic modeling of the sea floor," J. Acoust. Soc. Am. **68**, 1313–1340.

Heaney, K. D. (**2004a**). "Rapid geoacoustic characterization: Applied to range-dependent environments," IEEE J. Ocean. Eng. **29**, 43–50.

Heaney, K. D. (**2004b**). "Rapid geoacoustic characterization using a surface ship of opportunity," IEEE J. Ocean. Eng. **29**, 88–99.

Jensen, F. B., Kuperman, W. A., Porter, M. B., and Schmidt, H. (**2000**). *Computational Ocean Acoustics* (Springer-Verlag, New York), 580 p.

Mercer, J. A., Andrew, R. K., Howe, B. M., and Colosi, J. A. (**2005**). "Cruise report: Long-range ocean acoustic propagation experiment (LOAPEX)," Technical Report APL- UW TR0501, Applied Physics Laboratory, University of Washington, Seattle, WA.

Mercer, J. A., Colosi, J. A., Howe, B. M., Dzieciuch, M. A., Stephen, R., and Worcester, P. F. (**2009**). "LOAPEX: The long-range ocean acoustic propagation experiment," IEEE J. Ocean. Eng. **34**, 1–11.

Rypina, I. I., and Brown, M. G. (**2007**). "On the width of a ray," J. Acoust. Soc. Am. **122**, 1440–1448.

Sikora, J. J. (**2009**). "Sound propagation around underwater seamounts," Ph.D. thesis, Massachusetts Institute of Technology, MA.

Smith, W. H. F., and Sandwell, D. T. (**1997**). "Global seafloor topography from satellite altimetry and ship depth soundings," Science **277**, 1956–1962.

Stephen, R. A., Bolmer, S. T., Dzieciuch, M. A., Worcester, P. F., Andrew, R. K., Buck, L. J., Mercer, J. A., Colosi, J. A., and Howe, B. M. (**2009**). "Deep seafloor arrivals: An unexplained set of arrivals in long-range ocean acoustic propagation," J. Acoust. Soc. Am **126**, 599–606.

Stephen, R. A., Bolmer, S. T., Udovydchenkov, I. A., Worcester, P. F., Dzieciuch, M. A., Van Uffelen, L. J., Mercer, J. A., Andrew, R. K., Buck, L. J., Colosi, J. A., and Howe, B. M. (**2008**). "NPAL04 OBS data analysis part 1: Kinematics of deep seafloor arrivals," Technical Report WHOI-2008-3, Woods Hole Oceanographic Institution, Woods Hole, MA.

Stephen, R. A., Swift, S. A., and Greaves, R. J. (**1997**). "Bathymetry and sediment thickness survey of the Hawaii-2 cable," Technical Report WHOI-03-97, Woods Hole Oceanographic Institution, Woods Hole, MA.

Udovydchenkov, I. A. (**2007**). "Sound transmission through a fluctuating ocean: A modal approach," Ph.D. thesis, University of Miami, FL.

Udovydchenkov, I. A., Brown, M. G., Duda, T. F., Mercer, J. A., Andrew, R. K., Worcester, P. F., Dzieciuch, M. A., Howe, B. M., and Colosi, J. A. (**2012**). "Modal analysis of the range evolution of broadband wavefields in the North Pacific Ocean: Low mode numbers," J. Acoust. Soc. Am., **131**, 4409–4427.

Van Uffelen, L. J., Worcester, P. F., Dzieciuch, M. A., and Rudnick, D. L. (**2009**). "The vertical structure of shadow-zone arrivals at long range in the ocean," J. Acoust. Soc. Am. **125**, 3569–3588.

Van Uffelen, L. J., Worcester, P. F., Dzieciuch, M. A., Rudnick, D. L., and Colosi, J. A. (**2010**). "Effects of upper ocean sound-speed structure on deep acoustic shadow-zone arrivals at 500- and 1000-km range," J. Acoust. Soc. Am. **127**, 2169–2181.